

## ARTICLES

Anti-Jahn-Teller polaron in LaMnO<sub>3</sub>

Philip B. Allen and Vasili Perebeinos

*Department of Physics and Astronomy, State University of New York, Stony Brook, New York 11794-3800*

(Received 20 April 1999)

Distortions of the oxygen sublattice couple to  $e_g$  orbitals of  $Mn^{3+}$  and drive a cooperative Jahn-Teller (orbital ordering) transition in LaMnO<sub>3</sub>. A simple model for this transition is studied. Without further adjustment, the model predicts the shape and stability of small (anti-Jahn-Teller) polarons that form when holes are doped into the material. This leads to a new description of the lightly-doped insulator, the antiferromagnetic to ferromagnetic transition, and the metal-insulator transition. [S0163-1829(99)12639-0]

## I. INTRODUCTION

The doped manganites  $R_{1-x}S_xMnO_3$  (where  $R$  is typically La and  $S$  is typically Sr or Ca) have a fascinating  $(T, x)$  (temperature, concentration) phase diagram, including ‘‘colossal magnetoresistance’’<sup>1</sup> when  $T \approx 250$  K and  $x \approx 0.20$ . Experiment [transport,<sup>2</sup> optical,<sup>3</sup> diffraction,<sup>4</sup> extended x-ray-absorption fine structure (EXAFS),<sup>5</sup> isotope studies<sup>6</sup>] and theory<sup>7</sup> indicate the appearance of polarons at this point in  $(T, x)$ . It is less well appreciated that small polarons are essential to explain the insulating phase at smaller  $x$  and  $0 < T < 750$  K.<sup>8</sup> We study a simple model for the cooperative Jahn-Teller (JT) transition and use the model to predict properties of small polarons in lightly-doped material, including how they affect magnetic order and the metal-insulator transition. By working in the limit of large on-site Coulomb repulsion  $U$ , we find that properties of the polaron are simple enough to describe analytically, with small perturbative corrections.

There is disagreement over the relative role of Coulomb, magnetic, and electron-phonon effects. We offer a simple unified picture in which the relevant energy scales in descending order are (1) Coulomb interactions are inactive after establishing the dominant Hubbard and Hund energy scales; (2) electron-phonon interactions drive orbital ordering by the JT mechanism; (3) when doped, electron-phonon interactions via orbital ordering give small anti-JT polarons; and, finally, (4) orbital ordering disrupted by polarons is responsible for the unusual magnetic phases (described in Sec. III).

A canonical ‘‘Jahn-Teller polaron’’<sup>9</sup> is the excess electron in BaTiO<sub>3</sub>,<sup>10</sup> which sits in a triply degenerate  $t_{2g}$  level. A local distortion of the lattice splits the degenerate levels. Beyond a critical coupling strength, this lowers the energy and traps the electron in a small polaron state.

By contrast, the polarons in LaMnO<sub>3</sub> are ‘‘anti-JT polarons.’’ When pure, the valence is  $Mn^{3+}$ , with  $d^4$  configuration in the high-spin state  $t_{2g}^3 e_g^1$  with the doubly degenerate  $e_g$  level singly occupied. Below the JT structural transition at  $T_{JT} = 750$  K,<sup>11</sup> oxygen octahedra distort as illustrated schematically in Fig. 1, lifting the  $e_g$  degeneracy

and lowering the energy of the occupied orbitals. When a hole is added, we show that a small polaron is formed by locally ‘‘undoing’’<sup>8</sup> the JT distortion, pinning the hole onto a  $Mn^{4+}$  site with a filled  $t_{2g}$  shell.

## II. MODEL HAMILTONIAN

The Hamiltonian we use is  $\mathcal{H} = \mathcal{H}_t + \mathcal{H}_{ep} + \mathcal{H}_L + \mathcal{H}_U$ . The first term represents hopping of Mn  $e_g$  electrons to nearest neighbors. A simple way to derive this term is to introduce an overcomplete basis

$$\psi_x = 3x^2 - r^2, \quad \psi_y = 3y^2 - r^2, \quad \psi_z = 3z^2 - r^2, \quad (1)$$

each pointing toward the two nearest Mn neighbors along one of the Cartesian axes. Note that  $\psi_x + \psi_y + \psi_z = 0$ . In the two-dimensional  $e_g$  space, these basis vectors lie at  $120^\circ$  to each other, as shown in Fig. 2. The usual orthogonal basis,  $\psi_2 = (\psi_x - \psi_y)/\sqrt{3}$  and  $\psi_3 = \psi_z$ , is more complicated be-

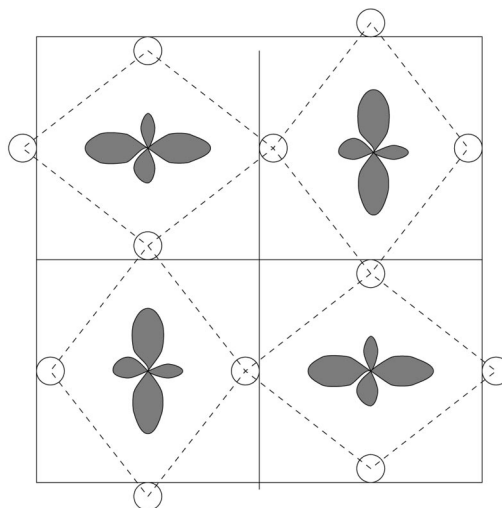


FIG. 1. Base plane ( $x$ - $y$  plane) of Jahn-Teller distorted LaMnO<sub>3</sub>. Rotations of oxygen octahedra are omitted, and distortions are exaggerated. Oxygens are displaced only along Mn-O-Mn bonds.

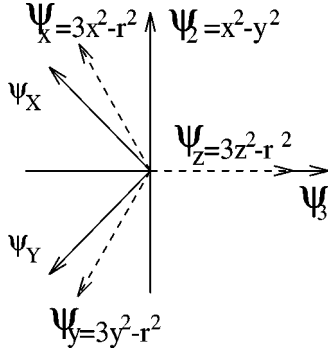


FIG. 2. The two-dimensional space of  $e_g$  orbitals, with vertical and horizontal axes being the usual orthogonal basis functions  $\psi_2$  and  $\psi_3$ . The symmetrical overcomplete basis functions  $\psi_x$ ,  $\psi_y$ , and  $\psi_z$ , Eq. (1), are shown as dashed lines, and the symmetrical orthogonal basis  $\psi_X$  and  $\psi_Y$ , Eq. (6), are shown lying at  $45^\circ$  in the second and third quadrants.

cause there is no element of the cubic rotation group that transforms  $\psi_2$  into  $\psi_3$ . Then for the hopping Hamiltonian we choose

$$\mathcal{H}_t = t \sum_{l, \pm} \{ [c_x^\dagger(l) c_x(l \pm \hat{x})] + [x \rightarrow y] + [y \rightarrow z] \}, \quad (2)$$

where  $l$  numbers manganese sites, and  $l + \hat{x}$  numbers the Mn neighbor to the right. After reexpressing  $\mathcal{H}_t$  in terms of the orthogonal orbitals  $\psi_2$  and  $\psi_3$ , we recover the correct nearest-neighbor two-center Slater-Koster<sup>12</sup> model, with overlap integrals  $t = (dd\sigma)$ ,  $(dd\pi)$  not entering due to symmetry, and  $(dd\delta) = 0$ .

The only lattice degree of freedom is oxygen motion along the direction of the bonds to the nearest two Mn atoms, with a harmonic restoring force  $-Ku_x$ . Variables  $Q_x(l) = u_x(l + \frac{1}{2}\hat{x}) - u_x(l - \frac{1}{2}\hat{x})$  measure the local expansion of oxygens on the  $x$  axis around the  $l$ th Mn atom. This expansion lowers the energy  $\epsilon_x$  of orbital  $\psi_x$  by  $\partial\epsilon_x/\partial Q_x = -4g/\sqrt{3}$ . We work in adiabatic approximation (oxygen mass is equal to  $\infty$ ). This gives

$$\mathcal{H}_{ep} = -\frac{4g}{\sqrt{3}} \sum_l \{ [c_x^\dagger(l) c_x(l) Q_x(l)] + [x \rightarrow y] + [y \rightarrow z] \}, \quad (3)$$

$$\mathcal{H}_L = \frac{K}{2} \sum_l [u_x(l + \frac{1}{2}\hat{x})^2 + u_y(l + \frac{1}{2}\hat{y})^2 + u_z(l + \frac{1}{2}\hat{z})^2]. \quad (4)$$

When two orbitals are occupied on one site, one has to pay Coulomb energy  $U$ :

$$\mathcal{H}_U = U \sum_l c_2^\dagger(l) c_2(l) c_3^\dagger(l) c_3(l). \quad (5)$$

We take into account  $t_{2g}$  spins, by defining the  $c^\dagger$  operators to create electrons whose spins (because of the large Hund's rule energy) are parallel to the  $S = 3/2$  core spin. Hopping [Eq. (2)] then operates only between adjacent Mn sites with parallel spins.

This model generalizes to  $e_g$  electrons the model of Rice and Sneddon<sup>13</sup> for  $s$  electrons in  $\text{BaBiO}_3$ . The same model, but with longer-range forces, was used by Millis<sup>14</sup> for  $\text{LaMnO}_3$ .

To analyze the solution, it is convenient to make a  $45^\circ$  rotation in  $(\psi_2, \psi_3)$  space, to a new orthogonal basis, shown by the solid arrows in Fig. 2,

$$\psi_X = \frac{1}{\sqrt{2}}(\psi_2 - \psi_3) = \frac{1}{\sqrt{6}}[(\sqrt{3} + 1)\psi_x + (\sqrt{3} - 1)\psi_y],$$

$$\psi_Y = -\frac{1}{\sqrt{2}}(\psi_2 + \psi_3) = \frac{1}{\sqrt{6}}[(\sqrt{3} - 1)\psi_x + (\sqrt{3} + 1)\psi_y]. \quad (6)$$

The orbitals  $\psi_X$  and  $\psi_Y$  point strongly in the  $\hat{x}$  and  $\hat{y}$  directions and are equivalent under a  $90^\circ$  rotation in real space, as shown in Fig. 1.

In the new basis the electron-phonon term in the Hamiltonian (3) is conveniently split into Jahn-Teller and breathing parts,  $\mathcal{H}_{ep} = \mathcal{H}_{JT} + \mathcal{H}_{br}$ :

$$\mathcal{H}_{JT} = -g \sum_l [c_X^\dagger(l), c_Y^\dagger(l)] \begin{pmatrix} Q_2(l) & Q_3(l) \\ Q_3(l) & -Q_2(l) \end{pmatrix} \begin{pmatrix} c_X(l) \\ c_Y(l) \end{pmatrix}, \quad (7)$$

$$\mathcal{H}_{br} = -\sqrt{2}(1 + \beta)g \sum_l Q_1(l) [c_X^\dagger(l) c_X(l) + c_Y^\dagger(l) c_Y(l)], \quad (8)$$

where the breathing amplitude is  $Q_1 = \sqrt{2/3}(Q_x + Q_y + Q_z)$ ,  $Q_2$  is  $Q_x - Q_y$ , and  $Q_3$  is  $(2Q_z - Q_x - Q_y)/\sqrt{3}$ , in standard Van Vleck<sup>15</sup> notation. A nonzero  $\beta$  was introduced by Millis to represent additional charge coupling to the breathing mode. To simplify the model, we use  $\beta = 0$ , which makes Eqs. (7) and (8) identical to Eq. (3).

The hopping Hamiltonian in the new basis is

$$\mathcal{H}_t = t \sum_{l, \delta=x,y,z} [c_X^\dagger(l), c_Y^\dagger(l)] T_\delta \begin{pmatrix} c_X(l \pm \delta) \\ c_Y(l \pm \delta) \end{pmatrix},$$

$$T_x = \begin{pmatrix} \frac{2 + \sqrt{3}}{4} & -\frac{1}{4} \\ -\frac{1}{4} & \frac{2 - \sqrt{3}}{4} \end{pmatrix}, \quad T_y = \begin{pmatrix} \frac{2 - \sqrt{3}}{4} & -\frac{1}{4} \\ -\frac{1}{4} & \frac{2 + \sqrt{3}}{4} \end{pmatrix},$$

$$T_z = \begin{pmatrix} \frac{1}{2} & \frac{1}{2} \\ \frac{1}{2} & \frac{1}{2} \end{pmatrix}. \quad (9)$$

### III. GROUND-STATE SOLUTION

We have solved this Hamiltonian for zero doping ( $x = 0$ ) in two opposite limits:  $U/t$  small, by a Hartree-Fock calculation, and  $U/t$  infinite. The two limits give similar answers. The latter case seems to us more realistic and has another advantage: since hopping is prevented by unit occu-

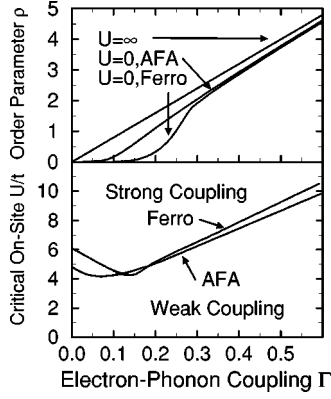


FIG. 3. Critical value of on-site repulsion  $U$ , which separates weakly-correlated from strongly-correlated solutions. The upper panel shows the Jahn-Teller distortion  $\rho = gu/t$  as a function of  $\Gamma = g^2/Kt$  for weak- and strong-coupling solutions.

pancy of all sites, the solution does not depend on the magnetic order. We postpone discussing the Hartree-Fock solution until the end of this section.

A distortion  $(Q_2, Q_3) = Q(\cos \theta, \sin \theta) \exp(i\vec{q} \cdot \vec{l})$  is introduced. We minimize elastic and electron energy to find optimal distortion parameters  $Q$ ,  $\theta$ , and  $\vec{q}$ . The optimal distortion has wave vector  $\vec{q} = (\pi, \pi, \pi)$ . Unless we add anharmonic or strain terms to select a direction in  $(Q_2, Q_3)$  space, the energy is independent of  $\theta$ . Experiment shows that the actual ordering is  $Q_2$  type, so we simply choose this distortion and avoid having an extra term in the Hamiltonian.

The ground electronic state that corresponds to perfect  $Q_2$ -type orbital order and  $U/t = \infty$  is

$$|\text{JT}\rangle = \prod_l^A c_X^\dagger(l) \prod_{l'}^B c_Y^\dagger(l') |0\rangle, \quad (10)$$

where  $A$  and  $B$  label sublattices where the phase of the orbital order  $\exp(i\vec{q} \cdot \vec{l})$  is  $\pm 1$ , respectively. The energy  $\langle \text{JT} | \mathcal{H} | \text{JT} \rangle = -NgQ + NKQ^2/16$  has minimum value  $E/N = -4\Gamma t$  at  $Q = 8g/K$  as shown in Fig. 3. This JT phase is insulating; the gap to charge excitations is approximately  $U \approx 6$  eV. Electron-phonon effects are conveniently expressed in terms of the dimensionless parameter  $\Gamma = g^2/Kt$ , which we estimate to be  $\approx 0.25-0.35$ . Orbital excitations<sup>16</sup> require only energy  $16\Gamma t \approx 2$  eV, and spin excitations occur down to low energies, with energies  $\approx 50$  K determined by balancing terms of order  $J \approx t^2/U$ .

As explained by Goodenough,<sup>11</sup> the  $Q_2$ -type orbital order (observed below  $T_{\text{JT}} = 750$  K) gives a layered structure (shown in Fig. 1) that in turn fixes the spin order which sets in below the Neel temperature  $T_N = 140$  K. The magnetic structure seen<sup>17</sup> at small  $x$  is ‘‘antiferromagnetic A’’ (AFA), with spins aligned ferromagnetically within the layers and antiferromagnetically perpendicular. The source of the ferromagnetic in-plane exchange [ $J_1 S^2 = 3.32$  meV (Ref. 18)] is orbital order, which favors virtual hops from filled  $A$  sublattice  $\psi_X$  orbitals to empty  $B$  sublattice  $\psi_X$  with spin parallel to avoid a Hund penalty. When orbitals are not ordered, the Hund penalty is outweighed by the greater multiplicity of hops, which  $t_{2g}$ -electrons can make onto empty  $t_{2g}$  states on

antiparallel neighbors. The antiferromagnetic  $c$ -axis exchange with  $J_2 S^2 = -2.32$  meV is explained this way.

It turns out that none of the energetics described so far (for  $Q_2$ -type orbital order) depend on the  $z$  component of the orbital ordering wave vector  $\vec{q}$ , which experimentally is  $(\pi, \pi, 0)$  rather than  $(\pi, \pi, \pi)$  as would be preferred for any orbital order other than pure  $Q_2$ . Again, we simply adopt this order without specifying the additional term in the Hamiltonian.

In the opposite limit  $U/t$  small, hopping energy is dominant, and the results depend on the magnetic order. We consider the two cases of ferromagnetic (ferro) and AFA order. In the latter case we turn off hopping in the  $z$  direction [ $T_z = 0$  in Eq. (9)]. Again, a distortion  $(Q_2, Q_3) = Q(\cos \theta, \sin \theta) \exp(i\vec{q} \cdot \vec{l})$  is introduced, and we minimize elastic and electron energy in Hartree-Fock (HF) approximation. At half-filling ( $x=0$ ) of the  $e_g$  bands, there is perfect nesting at wave vector  $\vec{q} = (\pi, \pi, \pi)$ , because of a symmetry of the bands of the undistorted crystal,  $\epsilon_1(\vec{k}) = -\epsilon_2(\vec{k} + \vec{q})$ . This fixes the optimal distortion at  $\vec{q} = (\pi, \pi, \pi)$ . The resulting HF energy is almost independent of the angle  $\theta$  in  $(Q_2, Q_3)$  space, favoring the  $Q_3$  distortion by one part in  $10^4$  of the JT energy. The calculations are shown in Fig. 3, which also shows the critical value of  $U/t$  at which the weak-coupling (HF) solution and the strong-coupling ( $U/t \rightarrow \infty$ ) solutions have equal total energy. For LaMnO<sub>3</sub>, we estimate  $U/t \approx 12$ . The lower panel of Fig. 3 shows that for this choice, the  $U \rightarrow \infty$  approximation is better. The upper panel shows that the JT distortion does not depend much on  $U$  for  $\Gamma \geq 0.25$ .

#### IV. SMALL POLARON

What happens when a hole is added? It can go into any of the states  $|lA\rangle$  and  $|l'B\rangle$  that are occupied in Eq. (10). When  $\Gamma = 0$ , the hole is free to hop among these states, no matter how large  $U$  is, since spins are aligned in the planes. When  $\Gamma > 0$ , it costs energy  $gQ = 8\Gamma t$  in lost JT energy to remove the electron. There are two different ways to regain some energy. (a) The hole can delocalize, forming a conducting Bloch state, with no relaxation of the oxygen coordinates  $Q(l)$ . For  $U = \infty$  the wave function in first approximation is

$$\psi_k = c_A \sum_l^A e^{ik \cdot \vec{l}} |lA\rangle + c_B \sum_{l'}^B e^{ik \cdot \vec{l}'} |l'B\rangle, \quad (11)$$

where the  $N$  states  $|lA\rangle, |l'B\rangle$  are obtained from  $|\text{JT}\rangle$  by putting the hole on a single site;  $|lA\rangle = c_X(l)|\text{JT}\rangle$  and  $|l'B\rangle = c_Y(l')|\text{JT}\rangle$ . The resulting hopping energy is  $\epsilon_k/t = (1/2)(\cos k_x + \cos k_y)$  plus an additional term  $-\cos k_z$  in the ferro case due to hopping in the  $z$  direction (prohibited in AFA case). The minimum energy of the extended hole state is  $E_{\text{h,ext}}/t = 8\Gamma - 1$  (AFA) and  $8\Gamma - 2$  (ferro). (b) If the distortions  $Q_l$  are locally readjusted, a bound state can be formed, which will be nonmetallic because a small impurity potential will pin it. In first approximation, put the hole at a single  $A$  site (neglecting hopping for now). The nearest  $\hat{x}$  oxygens, instead of being displaced outwards by  $u = 2g/K$ , should now displace inwards by  $u = -(\sqrt{4/3} - 1)g/K$ ; the  $\hat{y}$  oxygens, formerly displaced inwards by  $u = -2g/K$ , now

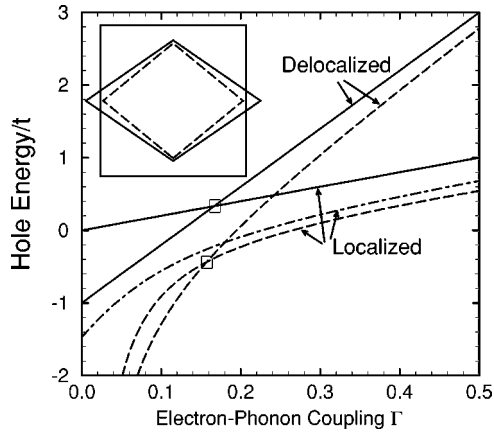


FIG. 4. Lowest hole energy in the AFA state of pure  $\text{LaMnO}_3$  as a function of coupling constant  $\Gamma$ , for the trial delocalized and localized solutions. Solid curves are lowest-order variational solutions, and dashed curves include perturbative corrections. The dash-dotted curve is an improved perturbative solution (exact subspace diagonalization) for the localized case. The crossover points at each level of approximation are shown in boxes. The inset shows (in exaggerated form) the shape of anti-Jahn-Teller polaron (dashed lines) in the  $x$ - $y$  plane. The relative positions of O atoms (at vertices of rhombus) in the pure JT (solid line) state and in the polaron state are accurate.

displace slightly further inwards, by  $u = -(\sqrt{4/3} + 1)g/K$ ; the  $\hat{z}$  neighbors, formerly undisplaced, now displace in by  $u = -\sqrt{4/3}g/K$ . The pattern of this anti-JT polaron is shown in Fig. 4. The energy  $E_{h,\text{pol}}/t$  needed to make the hole is reduced from  $8\Gamma$  in lost JT energy to  $2\Gamma$ . This energy comes partly from a reduction in the strain cost and partly from energy of breathing. Setting  $E_{h,\text{ext}} = E_{h,\text{pol}}$ , we conclude that small polarons are stable for  $\Gamma > 1/6$  in AFA phase and that ferromagnetism, by enhancing the delocalization energy, prevents small polarons until  $\Gamma > 1/3$ . These energies are shown as the solid curves in Fig. 4.

The three largest errors in the calculation of the hole energy are (1) the localized hole can spread somewhat onto neighboring Mn atoms, (2) the Hilbert space for both localized and delocalized hole wave functions should include states with orbital defects (sites occupied singly but by the orbital of wrong orientation), and (3) a hole in AFA phase will lower its energy further by causing spin canting on Mn atoms in adjacent planes, thus permitting interplanar hopping, and eventually driving an AFA to ferro transition. We have calculated these effects by perturbation theory. Details for processes (1) and (2) are given in the Appendix, and process (3) is further discussed in the next section.

The probability that a small hole polaron will be found away from the central site is  $a/(1.0366+a)$  where  $a = 0.0059/\Gamma^2$  (AFA) and  $0.0099/\Gamma^2$  (ferro). At the smallest  $\Gamma$  where small polarons are stable, the probability is 19% and 10%, respectively. This shows that the small polaron is very well localized. The first two effects cause the energy to be lowered by  $Ct\Gamma + C't/\Gamma$  with  $C=0$  for delocalized states and 0.49 for localized states, and  $C'=(0.11, 0.14)$ , in (AFA, ferro), for delocalized states and (0.11, 0.17) for localized. The shifts are small for values of  $\Gamma \geq 0.2$ . The critical value of  $\Gamma$  for small polaron formation changes from

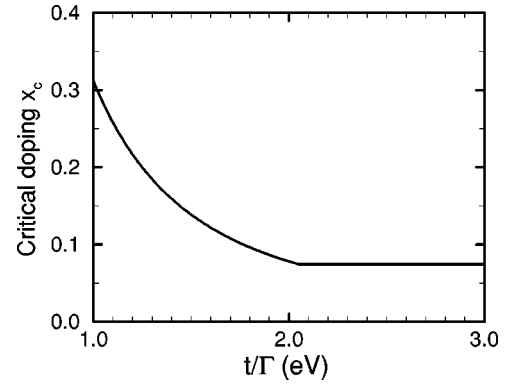


FIG. 5. Critical concentration  $x_c$  for the AFA to ferro transition as a function of coupling constants  $t/\Gamma$ .

$\Gamma_c = 1/6$  to 0.157 (AFA) and from  $1/3$  to 0.294 (ferro). The corrected energies are shown as the dashed curves in Fig. 4.

## V. MAGNETIC TRANSITION

Effect (3), the spin-canting problem, has usually been discussed on the assumption that holes are delocalized.<sup>19</sup> Treating spins classically, the additional delocalization energy gained when adjacent layers realign from  $180^\circ$  to  $180^\circ - \theta$  is  $t \sin(\theta/2)$  per hole; the exchange cost of realignment is  $J_2 S^2 [1 - \cos(\theta)]$  per Mn atom. The optimum canting angle is  $\sin(\theta/2) = xt/4|J_2|S^2$ , which gives a small critical concentration  $x_c = 4|J_2|S^2/t$  for complete rotation to the ferro phase. Localized holes tilt spins on only near-neighbor Mn atoms in adjacent planes, gaining less hopping energy than delocalized holes because the electron hops into an anti-JT-distorted hole site. The energy gain is  $(39/640)(t/\Gamma)\sin(\theta/2)$ . If we neglect the rotation of any spin except first-neighbor spins, the magnetic energy loss around the localized hole is  $(8J_1 + 2|J_2|)S^2[1 - \cos(\theta)]$  per hole, giving the optimum local rotation  $\sin(\theta/2) = 0.49 (\text{eV}^{-1})t/\Gamma$ . For  $t > 2.04\Gamma$  eV, the adjacent spins are completely flipped. Comparing the magnetic energy loss per spin to the energy loss of the ferro state, we find a critical concentration plotted in Fig. 5. Experimentally the AFA/ferro phase boundary occurs at  $x_c = 0.08$  for Sr-doped  $\text{LaMnO}_3$  (Ref. 20) and at  $x_c = 0.15$  for Ca doping.<sup>17</sup> These values are easily reconciled with the localized hole picture but demand too small a value of  $t$  in the delocalized picture. The smaller Ca ion causes larger Mn-O-Mn bond angles, which results in a smaller  $t$  and a larger  $x_c$ .

## VI. METAL-INSULATOR TRANSITION

At doping concentrations  $x$  approaching  $x_c = 0.20$ ,  $\text{LaMnO}_3$  becomes metallic. A possible analog system with simpler but similar physics is doped  $\text{BaBiO}_3$ . When Ba atoms are replaced by K atoms, the system remains insulating up to a concentration  $x = 0.40$ . The most likely and successful explanation for the insulating behavior is formation of bipolarons. The pure material has Bi atoms in the nominal  $\text{Bi}^{4+}$  valence state. Chemically, Bi prefers valences  $\text{Bi}^{3+}$  and  $\text{Bi}^{5+}$ . The pure material has alternating oxygen displacements inward or outward in the  $Q_1$  breathing pattern. This stabilizes charge ordering, which is interpretable as an alternation of  $\text{Bi}^{3+}$  and  $\text{Bi}^{5+}$ . When K atoms replace Ba,

extra electrons are released from Bi atoms, creating holes, and converting some of the Bi<sup>3+</sup> ions into Bi<sup>5+</sup>. The new Bi<sup>5+</sup> ions created by doping are small hole bipolarons, and are stabilized by relaxation of the  $Q_1$  coordinates of oxygens. A microscopic description has been given<sup>21</sup> using the Rice-Sneddon Hamiltonian,<sup>13</sup> which is just a simplified version of the Hamiltonian used here, with a single Bi  $s$  band in place of the two Mn  $e_g$  bands. The Hubbard  $U$  is much smaller for Bi  $s$  orbitals than for Mn  $e_g$ 's, so bipolarons are the stable defect of the Peierls-type charge-order parameter, while single polarons are the stable defect of the JT orbital order parameter of LaMnO<sub>3</sub>.

The metal-insulator transition in BaBiO<sub>3</sub> was addressed in a remarkable calculation by Yu, Chen, and Su<sup>22</sup> (verified by Kostur and Allen<sup>23</sup>). In their calculations, bipolaron defects form spontaneously in the Peierls order parameter up to very large concentrations, but when the concentration is too high, the defects destroy the Peierls order completely, and the ground state switches from defective dimerized insulator to undistorted metal. In the work of Kostur and Allen,<sup>23</sup> it is observed that the defective dimerized state (a ‘‘bipolaron glass’’ phase) is probably an Anderson insulator. The bipolarons are dense enough that localized single-particle states fill up the Peierls gap, and an Efros-Shklovskii pseudogap<sup>24</sup> rather than a clean gap separates the filled and empty states at the Fermi level. The insulating state might have a nonzero linear specific-heat coefficient  $\gamma$ . However, the metal-insulator transition is not an Anderson transition—the localized states do not persist away from the Fermi level in the metallic state but disappear altogether.

The transition in LaMnO<sub>3</sub> seems to us to be similar, with polarons instead of bipolarons, and JT rather than Peierls order being destroyed at the phase transition. We have not attempted a calculation, which would be more difficult for LaMnO<sub>3</sub> than for BaBiO<sub>3</sub> because of the large value of  $U$ . Schematically the energy of JT glass phase and metallic phase would possibly be

$$\begin{aligned} E_{\text{JT}}/Nt &= -[4 - a(U)x - b(U)x^2 + \dots]\Gamma, \\ E_{\text{metal}}/Nt &= -[c(U)x + d(U)x^2 + \dots], \end{aligned} \quad (12)$$

where coefficients  $a, b, c, d$ , etc. are unknown functions that depend strongly on  $U$  and also on the magnetic state. Our calculations above give the value of  $a$  at  $U = \infty$  to be 2 plus small corrections. If we could neglect  $bx$  relative to  $a$  and  $dx$  relative to  $c$ , then the critical concentration would be  $x_c = 4\Gamma/(a\Gamma + c)$ . The observed  $x_c \approx 0.2$  then requires that the hopping energy gain  $-ct$  in the correlated metal phase must be of order  $-5t$ , using  $\Gamma = 0.3$ , whereas we find that at  $U = 0$  the value of  $c$  in the ferromagnetic phase is only 3. This shows that the polaron repulsion  $b$  plays a significant role.

## VII. DISCUSSION

Numerous effects are left out of the model. Macroscopic strain, tilting of oxygen octahedra, and additional zero-point magnetic and nonadiabatic lattice fluctuations all could be added and would affect the  $T=0$  properties discussed here, but we believe that the effects we did include are the most important ones. A  $T>0$  treatment of all these effects is a bigger challenge. It would also be interesting to extend the

$T=0$  calculations to higher doping where a remarkable variety of textured phases is being unraveled.<sup>25</sup> The properties of LaMnO<sub>3</sub>-related materials are incredibly rich, yet surprisingly understandable, in contrast to certain other transition-metal oxide systems.

## ACKNOWLEDGMENTS

We thank W. Bao, M. Blume, D. E. Cox, J. P. Franck, J. B. Goodenough, J. P. Hill, D. I. Khomskii, and J.-S. Zhou for helpful conversations, and V. N. Kostur for technical guidance and for the inspiration to start the project. This work was supported in part by NSF Grant No. DMR-9725037.

## APPENDIX: PERTURBATIVE CORRECTIONS

In Sec. IV the energy of the hole in JT-distorted LaMnO<sub>3</sub> is computed in lowest order, for the two cases of localized and delocalized hole states. Here the method used for perturbative corrections is explained. First, we discuss the localized case.

Denoting the pure crystal ground state Eq. (10) as  $|\text{JT}\rangle$ , the strictly localized hole on an  $A$  site at the origin is  $c_X(0)|\text{JT}\rangle$ . For clarity, we use both a short-hand and a pictorial labeling scheme:

$$|h0\rangle = c_X(0)|\text{JT}\rangle = \left| \begin{array}{c} | \\ \text{O} \\ | \end{array} \right\rangle \quad (A1)$$

where  $h0$  means ‘‘hole at the origin.’’ This is the zeroth-order (unperturbed) state of the localized hole. As shown in Sec. IV, relaxation of oxygen positions reduces the energy  $\epsilon(h0) = \langle h0|\mathcal{H}_{\text{tot}}|h0\rangle$  from  $8\Gamma t$  to  $2\Gamma t$ . Our aim is to calculate the two corrections,

$$\delta E_1 = \sum_{i=1}^6 \frac{| \langle i|\mathcal{H}_{\text{JT}}|h0\rangle |^2}{\epsilon(h0) - \epsilon(i)}, \quad (A2)$$

$$\delta E_2 = \sum_{j=1}^{12} \frac{| \langle j|\mathcal{H}_t|h0\rangle |^2}{\epsilon(h0) - \epsilon(j)}. \quad (A3)$$

Included in the sums are all basis functions that couple to  $|h0\rangle$  by either  $\mathcal{H}_{\text{JT}}$  or  $\mathcal{H}_t$ . All our basis states have the same relaxed oxygen positions optimized for the  $|h0\rangle$  state.

The JT operator  $\mathcal{H}_{\text{JT}}$  couples  $|h0\rangle$  to six states  $|i\rangle$  with orbital defects on nearest-neighbor Mn atoms. The states  $|i\rangle$  come in three types. First, consider

$$|h0, o\hat{x}\rangle = c_X^\dagger(\hat{x})c_Y(\hat{x})c_X(0)|\text{JT}\rangle = \left| \begin{array}{c} | \\ \text{O} \\ - \end{array} \right\rangle \quad (A4)$$

and the related state  $|h0, o-\hat{x}\rangle$ . The label  $|h\hat{s}, o\hat{s}'\rangle$  has the meaning ‘‘hole at site  $\hat{s}$ , orbital defect at site  $\hat{s}'$ .’’ When there is no orbital defect, the second part of the label is omitted. These states have energy  $\epsilon(h0, o\pm\hat{x}) - \epsilon(h0) = (14 - 4/\sqrt{3})\Gamma t$ , reduced from the value  $16\Gamma t$  of a distant orbital defect by relaxation of the displaced oxygen lying between the origin and the  $\pm\hat{x}$  Mn. These states are coupled to  $|h0\rangle$  in first order by the  $\mathcal{H}_{\text{JT}}$  term proportional to  $Q_3(\pm\hat{x}) = -(2/3 + 1/\sqrt{3})g/K$ . Second are the states  $|h0, o\pm\hat{y}\rangle$

with the hole at the origin and the orbital defect at the  $\pm\hat{y}$  sites. These have a slightly increased energy denominator  $(14+4/\sqrt{3})\Gamma t$  and coupling amplitude to the  $|h0\rangle$  state caused by the oxygen relaxation  $Q_3(\pm\hat{y}) = -(2/3 - 1/\sqrt{3})g/K$ . Third, the states  $|h0, o \pm \hat{z}\rangle$  have the same energy denominator  $16\Gamma t$  as a distant orbital, because the only neighboring oxygen with an altered position lies along the  $\hat{z}$  axis, generating the term  $Q_3(\pm\hat{z}) = 4g/3K$ , which causes off-diagonal coupling. Adding the three types of corrections, we get the value for the first perturbative correction to the localized hole energy,

$$\delta E_1 = -\frac{628}{1287}\Gamma t \approx -0.488\Gamma t. \quad (\text{A5})$$

This correction is independent of magnetic ordering.

The hopping Hamiltonian  $\mathcal{H}_t$  couples state  $|h0\rangle$  to twelve states, which come in two categories of six each. One example of each category is

$$|h\hat{x}\rangle = c_Y(\hat{x})|JT\rangle = \begin{vmatrix} 1 & & \\ & 1 & \\ & & 0 \end{vmatrix} \quad (\text{A6})$$

$$|h\hat{x}, o0\rangle = c_Y^\dagger(0)c_X(0)c_Y(\hat{x})|JT\rangle = \begin{vmatrix} 1 & & \\ & 1 & \\ & & 0 \end{vmatrix}. \quad (\text{A7})$$

The first six have the hole displaced to a first-neighbor site, with the origin occupied by an electron in the ‘‘correct’’ orbital; the second six have a misoriented orbital at the origin. The hops without orbital defect in the  $\pm(\hat{x}, \hat{y})$  directions cost energy  $\epsilon(j) - \epsilon(h0) = 37\Gamma t/3$ , while the hops in the  $\pm\hat{z}$  direction (forbidden in the AFA magnetic state) cost  $40\Gamma t/3$ . Moving a hole to a remote site would cost slightly less energy  $12\Gamma t$ . Hops that leave an orbital defect at the origin cost an extra  $8\Gamma t$ . The coupling magnitude is determined by the off-diagonal part of the matrix of Eq. (9) for hopping without creating orbital defect at the origin and by the diagonal parts otherwise. The net result is

$$\delta E_2(\text{ferro}) = -\left(\frac{3}{148} + \frac{3}{80} + \frac{21}{244} + \frac{3}{128}\right)\frac{t}{\Gamma} \approx -0.167\frac{t}{\Gamma},$$

$$\delta E_2(\text{AFA}) = -\left(\frac{3}{148} + \frac{21}{244}\right)\frac{t}{\Gamma} \approx -0.106\frac{t}{\Gamma}. \quad (\text{A8})$$

These calculated shifts are shown in the AFA case as a dashed line in Fig. 4. The shifts are similar in magnitude to

the unperturbed energy. Therefore, we repeated the calculation with an exact diagonalization in the same subset of 18 states, which couple to  $|h0\rangle$ . The answer, shown as the dot-dashed line in Fig. 4, is not greatly different from the perturbative answer in the relevant regime of parameters.

In Sec. IV the case of the delocalized hole was treated by staying within the subspace of states  $c(l)|JT\rangle$  where  $c(l)$  removes an occupied JT orbital, and then diagonalizing the off-diagonal effects of  $\mathcal{H}_t$  by Fourier transformation to Bloch states. The hole is then put into the lowest-energy Bloch state. This calculation has omitted effects caused by the fact that  $\mathcal{H}_t$  also allows hops that leave behind a single orbital defect. We now correct for this perturbatively. Our Hilbert space has two subspaces. The Bloch states lie in the  $N$ -dimensional subspace with a single hole and no orbital defect. We must add a  $6N$ -dimensional space in which the hole has an orbital defect on an adjacent atom. These two subspaces are coupled by  $\mathcal{H}_t$ . The Schrödinger equation has the structure

$$\begin{pmatrix} \mathcal{H}_{JT} + \mathcal{H}_t - E & \mathcal{H}'_t \\ \mathcal{H}'_t & \mathcal{H}_{JT} - E \end{pmatrix} \begin{pmatrix} \psi_I \\ \psi_{II} \end{pmatrix} = 0. \quad (\text{A9})$$

Each element of the  $\psi_I$  subspace (no orbital defect) is coupled to six elements of the  $\psi_{II}$  subspace by hopping terms. The prime on  $\mathcal{H}'_t$  is used to designate the part of  $\mathcal{H}_t$  that creates an orbital defect. The JT energy is constant ( $8\Gamma t$  hole creation energy) in the  $\psi_I$  subspace and higher by the JT gap ( $16\Gamma t$ ) in the  $\psi_{II}$  subspace. In our perturbative treatment we leave out the off-diagonal effects of  $\mathcal{H}_t$  interior to the  $\psi_{II}$  subspace. The problem is then equivalent to an effective Hamiltonian

$$\mathcal{H}_{\text{eff}} = \mathcal{H}_{JT} + \mathcal{H}_t - \mathcal{H}'_t (\mathcal{H}_{JT} - E)^{-1} \mathcal{H}'_t \quad (\text{A10})$$

in the  $\psi_I$  subspace. Second-order perturbation theory uses the JT gap  $16\Gamma t$  as the energy denominator  $(\mathcal{H}_{JT} - E)$ . Then the last term in Eq. (A10) just gives a constant shift on the diagonal. The value depends on the magnetic state:

$$\delta E_3(\text{ferro}) = -\left(\frac{7}{64} + \frac{2}{64}\right)\frac{t}{\Gamma} \approx -0.141\frac{t}{\Gamma},$$

$$\delta E_3(\text{AFA}) = -\frac{7}{64}\frac{t}{\Gamma} \approx -0.109\frac{t}{\Gamma}. \quad (\text{A11})$$

This shift is shown as a dashed line (in the AFA case) in Fig. 4.

<sup>1</sup>G. Jonker and J. H. van Santen, *Physica (Amsterdam)* **16**, 337 (1950); *Colossal Magnetoresistance, Charge Ordering, and Related Properties of Manganese Oxides*, edited by C. N. R. Rao and B. Raveau (World Scientific, Singapore, 1998).

<sup>2</sup>M. Jaime, M. B. Salamon, M. Rubinstein, R. E. Treece, J. S. Horowitz, and D. B. Chrisey, *Phys. Rev. B* **54**, 11 914 (1996); T. T. M. Palstra, A. P. Ramirez, S-W. Cheong, B. R. Zegarski, P. Schiffer, and J. Zaanen, *ibid.* **56**, 5104 (1997); J. L. Cohn, J. J. Neumeier, C. P. Popoviciu, K. J. McClellan, and Th. Leventouri, *ibid.* **56**, R8495 (1997); D. C. Worledge, L. Miéville, and T. H. Geballe, *ibid.* **57**, 15 267 (1998); J. P. Franck, I. Isaac, W. Chen,

J. Chrzanowski, J. C. Irwin, and C. C. Homes, *J. Supercond.* **12**, 263 (1999).

<sup>3</sup>Y. Okimoto, T. Katsufuji, T. Ishikawa, A. Urushibara, T. Arima, and Y. Tokura, *Phys. Rev. Lett.* **75**, 109 (1995); K. H. Kim, J. H. Jung, and T. W. Noh, *ibid.* **81**, 1517 (1998); M. Quijada, J. Cerne, J. R. Simpson, H. D. Drew, K. H. Ahn, A. J. Millis, R. Shrekala, R. Ramesh, M. Rajeswari, and T. Venkatesan, *Phys. Rev. B* **58**, 16 093 (1998).

<sup>4</sup>S. L. Billinge, R. G. DiFrancesco, G. H. Kwei, J. J. Neumeier, and J. D. Thompson, *Phys. Rev. Lett.* **77**, 715 (1996); D. Louca, T. Egami, E. L. Brosha, H. Röder, and A. R. Bishop, *Phys. Rev.*

- B **56**, 8475 (1997).
- <sup>5</sup>T. A. Tyson, J. Mustre de Leon, S. D. Conradson, A. R. Bishop, J. J. Neumeier, H. Röder, and J. Zang, Phys. Rev. B **53**, 13 985 (1996); A. Lanzara, N. L. Saini, M. Brunelli, F. Natali, A. Bianconi, P. G. Radaelli, and S.-W. Cheong, Phys. Rev. Lett. **81**, 878 (1998).
- <sup>6</sup>G.-M. Zhao, K. Conder, H. Keller, and K. A. Müller, Nature (London) **381**, 676 (1996); J. P. Franck, I. Isaac, W. Chen, J. Chrzanowski, and J. C. Irwin, Phys. Rev. B **58**, 5189 (1998).
- <sup>7</sup>A. J. Millis, P. B. Littlewood, and B. I. Shraiman, Phys. Rev. Lett. **74**, 5144 (1995); A. J. Millis, B. I. Shraiman, and R. Mueller, Phys. Rev. Lett. **77**, 175 (1996); A. J. Millis, R. Mueller, and B. I. Shraiman, Phys. Rev. B **54**, 5389 (1996); **54**, 5405 (1996); H. Röder, J. Zang, and A. R. Bishop, Phys. Rev. Lett. **76**, 1356 (1996); J. D. Lee and B. I. Min, Phys. Rev. B **55**, 12 454 (1997).
- <sup>8</sup>Y. Yamada, O. Hino, S. Nohdo, R. Kanao, T. Inami, and S. Katano, Phys. Rev. Lett. **77**, 904 (1996).
- <sup>9</sup>K. H. Höck, H. Nickisch, and H. Thomas, Helv. Phys. Acta **56**, 237 (1983).
- <sup>10</sup>S. Köhne, O. F. Schirmer, H. Hesse, T. W. Kool, and V. Vikhnin, J. Supercond. **12**, 193 (1999).
- <sup>11</sup>J. B. Goodenough, A. Wold, R. J. Arnett, and N. Menyuk, Phys. Rev. **124**, 373 (1961); J. Rodriguez-Carvajal, M. Hennion, F. Moussa, A. H. Moudden, L. Pinsard, and A. Revcolevschi, Phys. Rev. B **57**, 3189 (1998); Y. Murakami, J. P. Hill, D. Gibbs, M. Blume, I. Koyama, M. Tanaka, H. Kawata, T. Arima, Y. Tokura, K. Hirota, and Y. Endoh, Phys. Rev. Lett. **81**, 582 (1998).
- <sup>12</sup>J. C. Slater and G. F. Koster, Phys. Rev. **94**, 1498 (1954).
- <sup>13</sup>T. M. Rice and L. Sneddon, Phys. Rev. Lett. **47**, 689 (1982).
- <sup>14</sup>A. J. Millis, Phys. Rev. B **53**, 8434 (1996).
- <sup>15</sup>J. H. Van Vleck, J. Chem. Phys. **7**, 72 (1939); J. Kanamori, J. Appl. Phys. **31**, 14S (1960); J. B. Goodenough, *Magnetism and the Chemical Bond* (Wiley Interscience, New York, 1963), p. 202; K. I. Kugel and D. I. Khomskii, Zh. Éksp. Teor. Fiz. **64**, 1429 (1973) [Sov. Phys. JETP **37**, 725 (1973)].
- <sup>16</sup>V. Perebeinos and P. B. Allen, Phys. Status Solidi B **215**, 607 (1995).
- <sup>17</sup>E. O. Wollan and W. C. Koehler, Phys. Rev. **100**, 545 (1955).
- <sup>18</sup>F. Moussa, M. Hennion, J. Rodriguez-Carvajal, H. Moudden, L. Pinsard, and A. Revcolevschi, Phys. Rev. B **54**, 15 149 (1996).
- <sup>19</sup>P. G. de Gennes, Phys. Rev. **118**, 141 (1960).
- <sup>20</sup>H. Kawano, R. Kajimoto, M. Kubota, and H. Yoshizawa, Phys. Rev. B **53**, 2202 (1996).
- <sup>21</sup>P. B. Allen and V. N. Kostur, Z. Phys. B: Condens. Matter **104**, 605 (1997).
- <sup>22</sup>J. Yu, X.-Y. Chen, and W. P. Su, Phys. Rev. B **41**, 344 (1990).
- <sup>23</sup>P. B. Allen and V. N. Kostur (unpublished).
- <sup>24</sup>A. L. Efros and B. I. Shklovskii, J. Phys. C **8**, L49 (1975); B. I. Shklovskii and A. L. Efros, *Electronic Properties of Doped Semiconductors* (Springer-Verlag, Berlin, 1984), Chap. 10.
- <sup>25</sup>W. Bao, J. D. Axe, C. H. Chen, and S.-W. Cheong, Phys. Rev. Lett. **78**, 543 (1997); P. G. Radaelli, D. E. Cox, M. Marezio, and S.-W. Cheong, Phys. Rev. B **55**, 3015 (1997); H. Kuwahara, Y. Moritomo, Y. Tomioka, A. Asamitsu, M. Kasai, R. Kumai, and Y. Tokura, *ibid.* **56**, 9386 (1997); S. Mori, C. H. Chen, and S.-W. Cheong, Nature (London) **392**, 473 (1998).